

Wigner crystal and bubble phases in graphene

C.-H. Zhang and Yogesh N. Joglekar

Department of Physics, Indiana University-Purdue University Indianapolis, Indianapolis, Indiana 46202, USA

(Dated: January 24, 2020)

Graphene, a single free-standing sheet of graphite with honeycomb lattice structure, is a semimetal with carriers that have linear dispersion. A consequence of this dispersion is the absence of Wigner crystallization in graphene, since the kinetic and potential energies both scale identically with density of carriers. We study the ground state of graphene in the presence of strong magnetic field focusing on states with broken translational symmetry. Our mean-field calculations show that at integer fillings a uniform state is preferred whereas at non-integer fillings, Wigner crystal states (with broken translational symmetry) have lower energy. We obtain the phase diagram of the system. We find that it is qualitatively similar to that of quantum Hall systems in semiconductor heterostructures. Our analysis predicts that non-uniform states, including Wigner crystal state, will occur in graphene in the presence of a magnetic field and will lead to anisotropic transport in high Landau levels.

PACS numbers: 73.22.-f, 73.20.Qt, 73.20.-r

I. INTRODUCTION

Two dimensional electron gas (2DEG), realized either in semiconductor heterostructures or by sprinkling electrons on Helium surface, has been extensively studied over the past few decades. It is known that such a system undergoes phase transition from a uniform state to a state with spontaneously broken translational symmetry, a Wigner crystal, when the carrier density is sufficiently low¹ or the temperature is sufficiently high.² In case of a 2DEG in semiconductors, this state occurs when the gain from lowering the potential energy by localization outweighs the kinetic energy cost associated with the localization *provided that the dispersion of carriers is well-described by an effective mass m^* , $E_k = \hbar^2 k^2 / 2m^*$* . This transition has been theoretically investigated,³ although unequivocal experimental evidence is still lacking. The spectrum of the electron gas changes radically in the presence of a strong magnetic field. The kinetic energy is quantized and each Landau level (the manifold of eigenstates with a given energy) has a macroscopic degeneracy. Since the kinetic energy is fixed for a given Landau level, it is possible to vary the ratio of potential energy and kinetic energy by changing the filling factor within a given Landau level, and the system undergoes a transition from a uniform state to states with broken translational symmetry. Indeed, this transition has been extensively studied theoretically.⁴ There is strong experimental evidence that the ground state of such a system at filling factors $\nu < 1/5$ is a Wigner crystal⁵ and that at partial filling factors in high Landau levels, the ground state is non-uniform.⁶ We remind the Reader that this evidence is obtained from transport measurements and that a direct measurement of spatial density modulation - crystalline structure - is exceedingly difficult since the 2DEG is buried under a substrate.

In this paper, we focus on how these results change when the carries in the 2D gas have a linear dispersion instead of the the usual effective-mass quadratic dispersion. Graphene, a single sheet of graphite with honeycomb lattice structure, is a realization of a system with such carriers. It has the added advantage that such a 2D gas of carriers is *not buried under a substrate* and is, therefore, amenable to local probes that can investigate the crystalline structure. Graphene is a semimetal in which the valance and conduction bands touch at two inequivalent points \mathbf{K} and $\mathbf{K}' = -\mathbf{K}$ (and four other points related by symmetry). In the vicinity of these points (valleys), the band structure of carriers is well described by $E_{\mathbf{k}} = \pm \hbar v_G k$ where $\hbar v_G = 5.8$ eV Å is the characteristic velocity and \mathbf{k} is measured from one of the six points at which the conduction and valance bands touch.^{7,8} Due to the linear dispersion of carriers in graphene, potential and kinetic energies both scale as $n^{3/2}$ with the carrier density n .Therefore, graphene does not undergo Wigner crystallization in the absence of an external magnetic field.⁹

In the presence of a magnetic field, however, the kinetic energy is quantized and its ratio with the potential energy can be varied by changing the filling factor. This raises the prospect of Wigner crystal states in graphene. Here, we present a systematic mean-field analysis of the ground state of graphene in the quantum Hall regime, focusing on partial filling of the first few Landau levels. The plan for the paper is as follows. In the next section, we set up the low-energy Hamiltonian for graphene in the presence of magnetic field and recall results for the single-particle spectrum. In Sec. III, we set up the formalism for Hartree-Fock mean-field approximation and discuss its details. In Sec. IV, we present the numerical results we obtain. We discuss the phase diagram of graphene as a function of the partial filling factor and the density profiles. We find that the results closely follow those of non-uniform states in the conventional 2DEG. We end the paper with a brief discussion and conclusions in section V.

II. GRAPHENE IN MAGNETIC FIELD

The low-energy Hamiltonian for electrons in the \mathbf{K} valley is given by^{10,11}

$$H_{\mathbf{K}} = v_G (p_x \tau_x + p_y \tau_y^*), \quad (1)$$

where τ_x and τ_y are Pauli matrices in the space consisting of two lattice sites A and B within a single unit cell (The Hamiltonian for the other valley is obtained by complex conjugation). The Hamiltonian in the presence of an magnetic field is obtained by Peirels substitution $\mathbf{p} \rightarrow \mathbf{p} - e\mathbf{A}/c$. In a uniform magnetic field $\mathbf{B} = B\hat{z}$, generated by a vector potential $\mathbf{A} = Bx\hat{y}$, the Hamiltonian (1) becomes

$$H_{\mathbf{K}} = \frac{\sqrt{2}\hbar v_G}{l_B} \begin{pmatrix} 0 & c_k \\ c_k^\dagger & 0 \end{pmatrix}, \quad (2)$$

where $c_k = -i[l_B \partial_x + (x/l_B - kl_B)]/\sqrt{2}$ is the lowering operator, $l_B = \sqrt{\hbar c/eB}$ is the magnetic length, and $[c_k, c_k^\dagger] = 1$. The eigenvalues of this Hamiltonian are given by $E_n = \pm \hbar v_G \sqrt{2|n|}/l_B$ and the corresponding eigenfunctions are given by

$$\langle \mathbf{r} | \mathbf{K}, nk \rangle = \frac{1}{\sqrt{2L_y}} e^{iky} \begin{bmatrix} \text{sgn}(n) \varphi_{|n|-1}(x - kl_B^2) \\ \varphi_{|n|}(x - kl_B^2) \end{bmatrix} \quad (3)$$

for $n \neq 0$ and

$$\langle \mathbf{r} | \mathbf{K}, 0k \rangle = \frac{1}{\sqrt{L_y}} e^{iky} \begin{bmatrix} 0 \\ \varphi_0(x - kl_B^2) \end{bmatrix} \quad (4)$$

for $n = 0$. Here, $\varphi_n(x)$ are the simple harmonic oscillator eigenfunctions defined by $\varphi_n(x) = \langle x | (c_k^\dagger)^n | 0 \rangle / \sqrt{n!}$ and L_y is the sample length in y -direction. (In the following, we will use units such that $l_B = 1$). Thus, $n = 0$ eigenfunctions in graphene are identical to $n = 0$ states in a conventional 2DEG, whereas for $n \neq 0$, the eigenfunctions of graphene are an admixture of wavefunctions on the A and B lattice sites.¹² Therefore, we expect that graphene, like conventional 2DEG at partial filling factors, will support non-uniform (Wigner crystal) states.

In the following, we denote crystals with one electron per unit cell, $N_e = 1$ as Wigner crystals, and those with $N_e \geq 2$ per unit cell as bubble crystals. We also consider modulated stripe states that can be described by oblique, rectangular, or centered rectangular lattices.^{13,14} We call these states anisotropic Wigner crystals, and the ones having a triangular or square lattice structure as isotropic Wigner crystals. For simplicity, we assume that each Landau level in graphene is two-fold degenerate (valley degeneracy) and that the electron spins are fully polarized.

III. HARTREE-FOCK MEAN-FIELD HAMILTONIAN

The microscopic Hamiltonian for carriers in graphene consists of the kinetic energy and Coulomb repulsion. We use a pseudospin notation to denote the valley index: $\sigma = +$ corresponds to the \mathbf{K} valley and $\sigma = -$ corresponds to the $\mathbf{K}' = -\mathbf{K}$ valley. In the single-particle basis (3,4) the Hamiltonian is

$$\hat{H} = N_\phi \sum_{n\sigma} (E_n - \mu) \hat{\rho}_n^{\sigma,\sigma}(0) + \frac{N_\phi}{4\pi l_B^2} \sum_{\mathbf{q}, \{\sigma n\}} V(\mathbf{q}) \mathcal{F}_{n_1, n_4}(\mathbf{q}) \mathcal{F}_{n_2, n_3}(-\mathbf{q}) \hat{\rho}_{n_1, n_4}^{\sigma_1, \sigma_1}(-\mathbf{q}) \hat{\rho}_{n_2, n_3}^{\sigma_2, \sigma_2}(\mathbf{q}), \quad (5)$$

where $N_\phi = A/(2\pi l_B^2)$ is the number of flux quanta in the area A of the sample, μ is the chemical potential, $V(\mathbf{q}) = 2\pi e^2/\epsilon q$ is the Coulomb interaction and ϵ is the dielectric constant of graphene ($\epsilon \sim 3$), $\hat{\rho}_{n,n'}^{\sigma,\sigma'}(\mathbf{q})$ is the density matrix element defined as

$$\hat{\rho}_{n,n'}^{\sigma,\sigma'}(\mathbf{q}) = \frac{1}{N_\phi} \sum_{kk'} e^{-\frac{i}{2}q_x(k+k')l_B^2} c_{\sigma nk}^\dagger c_{\sigma n' k'} \delta_{k,k'+q_y} \quad (6)$$

with $c_{\sigma nk}^\dagger$ ($c_{\sigma nk}$) the creation (annihilation) operator of the electrons, $\mathcal{F}_{nn'}(\mathbf{q})$ is the form factor

$$\mathcal{F}_{n_1, n_2}(\mathbf{q}) = \frac{1}{2} [(1 + \delta_{n_1, 0} \delta_{n_2, 0}) F_{n_1, n_2}(\mathbf{q}) + \text{sgn}(n_1 n_2) F_{n_1-1, n_2-1}(\mathbf{q})]. \quad (7)$$

This form factor is the linear combination of the form factors for wave functions on lattice sites A and B ,

$$F_{n_1 \geq n_2}(\mathbf{q}) = \sqrt{\frac{|n_2|!}{|n_1|!}} \left[\frac{(-q_y + iq_x)}{\sqrt{2}} \right]^{(|n_1| - |n_2|)} L_{|n_2|}^{|n_1| - |n_2|} \left(\frac{q^2}{2} \right) e^{-q^2/4} \quad (8)$$

and $F_{n_1 \leq n_2}(\mathbf{q}) = F_{n_2, n_1}(-\mathbf{q})^*$. Here $L_n^m(x)$ is the generalized Laguerre polynomial. To obtain the Hamiltonian (5), we have ignored the interaction terms that scatter electrons from one valley to another and are exponentially and algebraically small in a/l_B where a is the lattice constant of graphene ($a \sim 5 \text{ \AA}$, $l_B \sim 100 \text{ \AA}$).¹⁵

The derivation of the Hartree-Fock mean-field Hamiltonian from Eq. (5) is straightforward and has been discussed extensively in the literature.^{16,17,18} When inter-Landau level transitions are ignored, the mean-field Hamiltonian contains a single Landau level index and is given by

$$H_{HF} = \frac{N_\phi e^2}{\epsilon l_B} \sum_{\sigma \mathbf{Q}} \left\{ \left[\frac{(E_n - \mu)}{e^2/\epsilon l_B} \delta_{\mathbf{Q},0} + H_n(\mathbf{Q}) - X_n^{\sigma, \sigma}(\mathbf{Q}) \right] \hat{\rho}_n^{\sigma, \sigma}(\mathbf{Q}) - X_n^{\sigma, \bar{\sigma}}(\mathbf{Q}) \hat{\rho}_n^{\bar{\sigma}, \sigma}(\mathbf{Q}) \right\} \quad (9)$$

where \mathbf{Q} is a reciprocal lattice vector of the Wigner crystal and $\bar{\sigma} = -\sigma$. The dimensionless Hartree and Fock potentials are given by

$$H_n(\mathbf{Q}) = \frac{e^{-Q^2/2}}{Q} |\mathcal{F}_{n,n}(\mathbf{Q})|^2 \rho_n(-\mathbf{Q}) (1 - \delta_{\mathbf{Q},0}), \quad (10)$$

$$X_n^{\sigma, \sigma'}(\mathbf{Q}) = \int_0^\infty dx e^{-x^2/2} |\mathcal{F}_{n,n}(x)|^2 J_0(xQ) \rho_n^{\sigma, \sigma'}(-\mathbf{Q}) \quad (11)$$

where $\rho_n^{\sigma, \sigma'}(\mathbf{Q}) = \langle \hat{\rho}_{n,n}^{\sigma, \sigma'}(\mathbf{Q}) \rangle$ are determined self-consistently from the mean-field Hamiltonian (9) and $\rho_n(\mathbf{Q}) = \sum_{\sigma=\pm} \rho_n^{\sigma, \sigma}(\mathbf{Q})$ is the total density at wavevector \mathbf{Q} .

The density matrix $\rho_n^{\sigma, \sigma'}(\mathbf{Q})$ is determined from the equal-time limit ($\tau \rightarrow 0^-$) of the single-particle Green's function

$$G_n^{\sigma, \sigma}(k_1, k_2; \tau) = -\langle \text{Tr} c_{nk_1\sigma}(\tau) c_{nk_2\sigma'}^\dagger(0) \rangle. \quad (12)$$

We define the Fourier transform of $G_n^{\sigma, \sigma'}(k_1, k_2; \tau)$ as

$$G_n^{\sigma, \sigma'}(\mathbf{Q}, i\omega_m) = \frac{1}{N_\phi} \sum_{k_1 k_2} \int_0^\beta d\tau e^{-iQ_x(k_1+k_2)/2 + i\omega_m \tau} \delta_{k_2, k_1 - Q_y} G_n^{\sigma, \sigma'}(k_1, k_2; \tau) \quad (13)$$

where $\beta = 1/k_B T$ is the inverse temperature. The equation of motion for $G_n^{\sigma, \sigma'}(\mathbf{Q}, i\omega_m)$ is given by^{17,18}

$$\begin{bmatrix} \delta_{\mathbf{Q},0} \\ 0 \end{bmatrix} = (i\omega_m + \mu) \begin{bmatrix} G_n^{+,+}(\mathbf{Q}, i\omega_m) & G_n^{+,-}(\mathbf{Q}, i\omega_m) \\ G_n^{-,+}(\mathbf{Q}, i\omega_m) & G_n^{-,-}(\mathbf{Q}, i\omega_m) \end{bmatrix} - \sum_{\mathbf{Q}'} \begin{bmatrix} \Sigma_n^{+,+}(\mathbf{Q}, \mathbf{Q}') & \Sigma_n^{+,-}(\mathbf{Q}, \mathbf{Q}') \\ \Sigma_n^{-,+}(\mathbf{Q}, \mathbf{Q}') & \Sigma_n^{-,-}(\mathbf{Q}, \mathbf{Q}') \end{bmatrix} \begin{bmatrix} G_n^{+,+}(\mathbf{Q}', i\omega_m) \\ G_n^{-,+}(\mathbf{Q}', i\omega_m) \end{bmatrix} \quad (14)$$

where the Hartree and exchange self-energy terms are given by

$$\Sigma_n^{\sigma, \sigma}(\mathbf{Q}, \mathbf{Q}') = [H_n(\mathbf{Q}' - \mathbf{Q}) - X_n^{\sigma, \sigma}(\mathbf{Q}' - \mathbf{Q})] \exp\left(\frac{i}{2} \mathbf{Q} \times \mathbf{Q}' \cdot \hat{z}\right), \quad (15)$$

$$\Sigma_n^{\sigma, \bar{\sigma}}(\mathbf{Q}, \mathbf{Q}') = -X_n^{\sigma, \bar{\sigma}}(\mathbf{Q}' - \mathbf{Q}) \exp\left(\frac{i}{2} \mathbf{Q} \times \mathbf{Q}' \cdot \hat{z}\right) \quad (16)$$

and $\mathbf{Q} \times \mathbf{Q}' \cdot z = Q_x Q'_y - Q_y Q'_x$. In order to solve Eq.(14), we diagonalize the self-energy matrix

$$\sum_{\mathbf{Q}'} \begin{bmatrix} \Sigma_n^{+,+}(\mathbf{Q}, \mathbf{Q}') & \Sigma_n^{+,-}(\mathbf{Q}, \mathbf{Q}') \\ \Sigma_n^{-,+}(\mathbf{Q}, \mathbf{Q}') & \Sigma_n^{-,-}(\mathbf{Q}, \mathbf{Q}') \end{bmatrix} \begin{bmatrix} V_j(\mathbf{Q}') \\ U_j(\mathbf{Q}') \end{bmatrix} = \omega_j \begin{bmatrix} V_j(\mathbf{Q}) \\ U_j(\mathbf{Q}) \end{bmatrix} \quad (17)$$

in a basis with a specific lattice structure, where (V_j, U_j) is the j -th eigenvector and ω_j is its corresponding eigenvalue. Using these eigenvectors and eigenvalues, one can calculate the density matrix

$$\begin{bmatrix} \rho_n^{+,+}(\mathbf{Q}) & \rho_n^{+,-}(\mathbf{Q}) \\ \rho_n^{-,+}(\mathbf{Q}) & \rho_n^{-,-}(\mathbf{Q}) \end{bmatrix} = \sum_j [V_j^*(0), U_j^*(0)] \begin{bmatrix} V_j(\mathbf{Q}) \\ U_j(\mathbf{Q}) \end{bmatrix} f(\omega_j - \mu) \quad (18)$$

where $f(\omega - \mu)$ is the Fermi-Dirac distribution function and the chemical potential μ is determined by

$$\rho_n^{+,+}(0) = \sum_j V_j(0) V_j^*(0) f(\omega_j - \mu) = \frac{1}{2} \nu. \quad (19)$$

We solve the set of equations (14-19) self-consistently to obtain the resultant density matrix and the ground state energy per particle for different lattice structures. The real-space density profile is then obtained using inverse Fourier transform,

$$n(\mathbf{r}) = \frac{1}{2\pi l_B^2} \sum_{\sigma\mathbf{Q}} \rho_n^{\sigma,\sigma}(\mathbf{Q}) \mathcal{F}_{n,n}(\mathbf{Q}) e^{i\mathbf{Q}\cdot\mathbf{r}} \quad (20)$$

For simplicity, in the numerical results for density profile, we use the dimensionless density, $2\pi l_B^2 n(\mathbf{r})$.

IV. NUMERICAL RESULTS

Now we turn to the numerical results. It follows from Eq. (9) that a state with intervalley coherence always has lower energy than a state without the coherence. Therefore, we only focus on solutions with $\rho_n^{+,+} \neq 0$. Thus, the ground state consists of electrons occupying the symmetric state (between the two valleys) when the filling factor within a Landau level is $\nu < 1$. We use a simplified oblique lattice with two primitive lattice vectors¹⁹ $\mathbf{a}_1 = (a, b/2)$, $\mathbf{a}_2 = (0, b)$ ((We perform similar analysis with square, rectangular, and centered rectangular lattices, and obtain results similar to those presented below). We denote the ratio $\gamma = b/a$. Note that the triangular lattice ($\gamma = 2/\sqrt{3}$) and quasi-striped states ($\gamma \rightarrow 0$) are its special cases. We do not consider purely one-dimensional striped states because they are prone to density modulations along the stripes.¹³ The two lattice constants are determined by the constraint that the unit cell contain N_e electrons, and are given by $a = l_B \sqrt{2\pi N_e / \nu \gamma}$ and $b = a\gamma$. The reciprocal lattice basis vectors are

$$\mathbf{b}_1 = \frac{2\pi}{a} (1, 0), \quad \mathbf{b}_2 = \frac{2\pi}{a} \left(-\frac{1}{2}, \frac{1}{\gamma} \right), \quad (21)$$

and the reciprocal lattice vectors are given by $\mathbf{Q}_{mn} = m\mathbf{b}_1 + n\mathbf{b}_2$. We determine the optimal lattice structure by obtaining the γ ($0 < \gamma \leq 2/\sqrt{3}$) that minimizes the mean-field energy. We use an external (infinitesimal) potential with the symmetry of the lattice to generate the initial density matrix,

$$\Sigma_{ex}(\mathbf{Q}, \mathbf{Q}') = -\exp \left[-\frac{Q_0^2}{2} - \frac{1}{4} (Q^2 + Q'^2) + \frac{1}{2} (\mathbf{Q} \cdot \mathbf{Q}' + i\mathbf{Q} \times \mathbf{Q}' \cdot \hat{z}) \right] \quad (22)$$

where $Q_0 = |\mathbf{Q}_{11}|$. We adjust the number of basis states used to calculate the density matrix, and verify that the zero-temperature sum rule¹⁷

$$\sum_{\mathbf{Q}} [|\rho_n^{+,+}(\mathbf{Q})|^2 + |\rho_n^{+,-}(\mathbf{Q})|^2] = \rho_n^{+,+}(0) \quad (23)$$

is satisfied within an accuracy of 10^{-5} .

For $n = 0$, the equivalence between single-particle wavefunctions for graphene and conventional 2DEG, implies that at small filling factors, the ground state is a triangular Wigner crystal.²⁰ Indeed, graphene, with its pseudospin (valley index) can be mapped onto a bilayer system in which layer index is the pseudospin, in the limit when the layer separation $d \rightarrow 0$. Our calculations, reproduce the results for ground state energy and lattice structure. Figure 1 shows the mean-field energy per particle (phase diagram) as a function of partial filling factor for different lattice structures. We see that for $\nu \leq 0.62$, the ground state is triangular Wigner crystal; it becomes an anisotropic Wigner crystal for $\nu \geq 0.62$. We find that a bubble crystal with $N_e = 3$ is identical, in energy, to the triangular Wigner crystal, and the bubble crystals with $N_e \geq 2$ have higher energies. Figure 2 shows the real-space electron density profile for graphene at partial filling $\nu = 0.25$ and for a bilayer quantum Hall system at layer separation $d = 0$ at the same filling factor. We obtain, as expected, identical density profiles with a triangular Wigner crystal. As the partial filling ν is increased, the ground state of the system changes to an anisotropic Wigner crystal (Figure 3). We find, in general, that the optimal value of anisotropy is high. Therefore the electron density resembles uniform stripe states and the density modulation along the stripes is quite small (Figure 3).

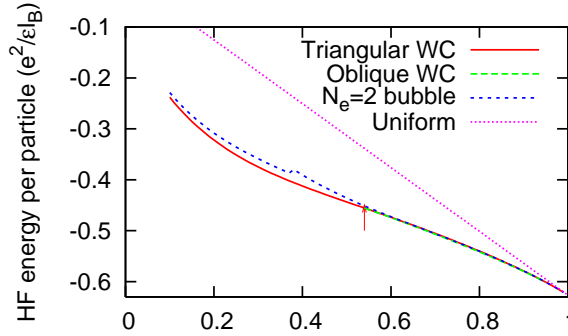


FIG. 1: (Color Online) Ground state energy per particle (measured in units of e^2/ϵ_B) in graphene as a function of partial filling ν in the $n = 0$ Landau level. The ground state is a triangular Wigner crystal for small ν and becomes an anisotropic Wigner crystal as ν increases. The arrow mark critical filling factors ν^* at which transition from the triangular Wigner crystal to the anisotropic Wigner crystal takes place. Note that for $n = 0$, the bubble crystal always has higher energy.

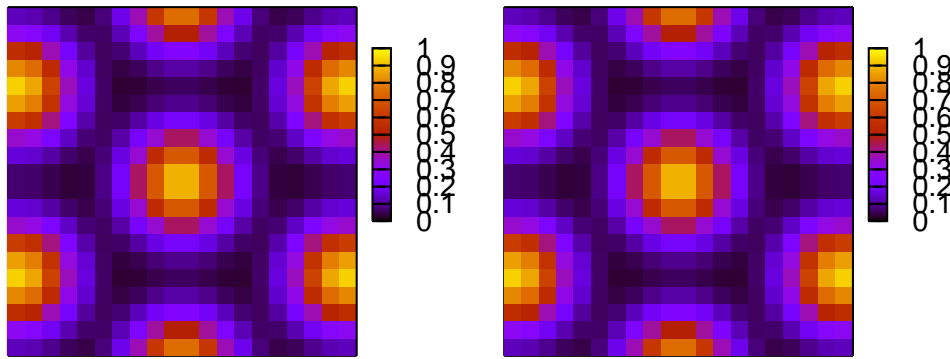


FIG. 2: (Color Online) A density plot of the ground state electron density in graphene (left) and a bilayer system with $d = 0$ (right) in the $n = 0$ Landau level with partial filling $\nu = 0.25$. According to the phase diagram in Fig. 1, the ground state is an isotropic triangular crystal. As expected, due to the equivalence between the two systems in the $n = 0$ Landau level, the two densities are identical.

For $n \geq 1$, the equivalence between graphene and a bilayer quantum Hall system at layer separation $d = 0$ breaks down since the single-particle wave functions are different. Figures 4-6 show the phase diagram as a function of partial filling factor ν for Landau levels $n=1-3$, respectively. The phase diagram of $n = 1$ Landau level is qualitatively similar to $n = 0$ Landau level. For $n \geq 2$ we find that the ground state for graphene is an isotropic crystal when the partial filling factor ν is small, whereas it is an anisotropic crystal when ν is sufficiently large. For intermediate values of ν , we find that the ground state is a bubble crystal with $N_e = 2$ or $N_e = 3$. For example, for $n = 2$ Landau level in graphene, the triangular Wigner crystal is stable for $\nu \leq 0.28$, the bubble state with two electrons $N_e = 2$ is stable for $0.28 \leq \nu \leq 0.43$, whereas for $\nu \geq 0.43$ an anisotropic Wigner crystal has the lowest energy. We can also see that the critical values of ν at which transitions from a triangular Wigner crystal to a bubble state to an anisotropic Wigner crystal take place are systematically higher than corresponding values for a bilayer system at $d = 0$. Figure 7 shows optimal value of $\gamma(\nu)$ for the ground state crystal structure for different Landau level indices. We see that the transition from an isotropic Wigner crystal ($\gamma = 2/\sqrt{3} = 1.15$) to an anisotropic Wigner crystal in graphene (a) occurs at higher values of ν than the corresponding values in bilayer systems (b).

Figure 8 shows the (dimensionless) real-space electron density profile for the $n = 3$ Landau level when the system is in the isotropic Wigner crystal state ($\nu = 0.18$), in the bubble crystal state with $N_e = 2$ ($\nu = 0.25$) and with $N_e = 3$ ($\nu = 0.35$), and in the anisotropic Wigner crystal state ($\nu = 0.75$). We see that the density profile is different from that in the lowest Landau level, due to different form factors. It is instructive to compare density profiles of the anisotropic Wigner crystal in the $n = 3$ Landau level and $n = 0$ Landau level (Fig. 3). We see that both resemble a (quasi)-uniform striped states, although the $n = 3$ density profile also shows the existence of uniform stripes between the modulated ones.

We end this section by comparing the electron density profiles in graphene and bilayer system with $d = 0$ at partial filling $\nu = 0.25$ in the $n = 1$ Landau level in Fig. 9. Recall that in the lowest Landau level, these density profiles are identical (Fig 2). For both systems, the self-consistent solutions for the density matrix $\rho_n^{\sigma\sigma'}(\mathbf{q})$ are identical; however,

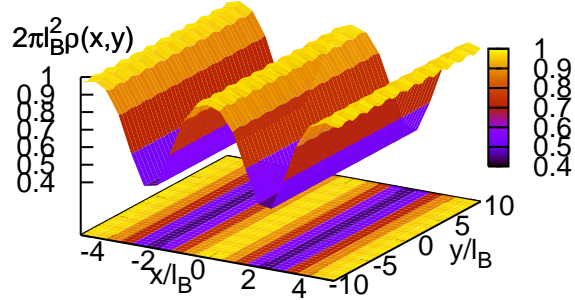


FIG. 3: (Color Online). Electron density profile for the anisotropic Wigner crystal ground state at $\nu = 0.75$ in the lowest Landau level. Notice that the density modulation along the y -axis is small and the system behaves essentially like a striped state.

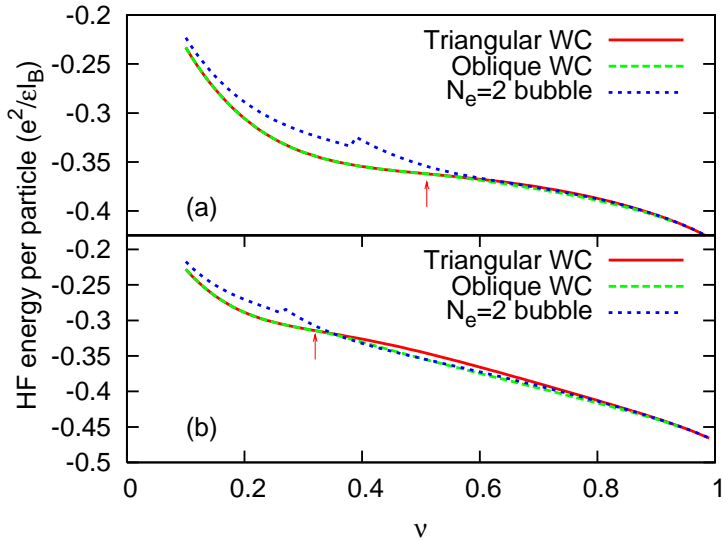


FIG. 4: (Color Online) Ground state energy per particle (measured in units of e^2/ϵ_B) for different crystal structures in the $n = 1$ Landau level for (a) graphene, and (b) a bilayer system at $d = 0$. The arrows mark the critical filling factor ν^* at which transition from the triangular Wigner crystal to anisotropic Wigner crystal takes place.

for $n \geq 1$, due to the differences in form factors, the resultant real-space electron density profiles are different.

V. DISCUSSION AND CONCLUSIONS

In this paper, we have systematically studied the ground state of graphene in the presence of a strong magnetic field, focusing on broken symmetry states with intervalley coherence, using the Hartree-Fock mean-field analysis. We have ignored the inter-Landau level transitions and focused only states with inter-valley coherence because, due to the isotropic nature of the Coulomb interaction in the pseudospin space, energy of a state without coherence is always larger than the energy of a state with coherence. Our calculations, naturally, have also not taken into account competing fluid states, such as the Laughlin state, with uniform density. Such fluid states will have lower energy at special value of filling factor (for example, $\nu = 1/3$); however, our results likely represent the true ground state of the system at generic filling factors and in high Landau levels (where, in a conventional 2DEG, Hartree-Fock mean-field solutions are reliable).

Our analysis found that since the kinetic energy of graphene's linearly dispersing carriers is quenched in the presence of a magnetic field, graphene is qualitatively similar to a conventional 2DEG with a quantum degree of freedom (bilayer

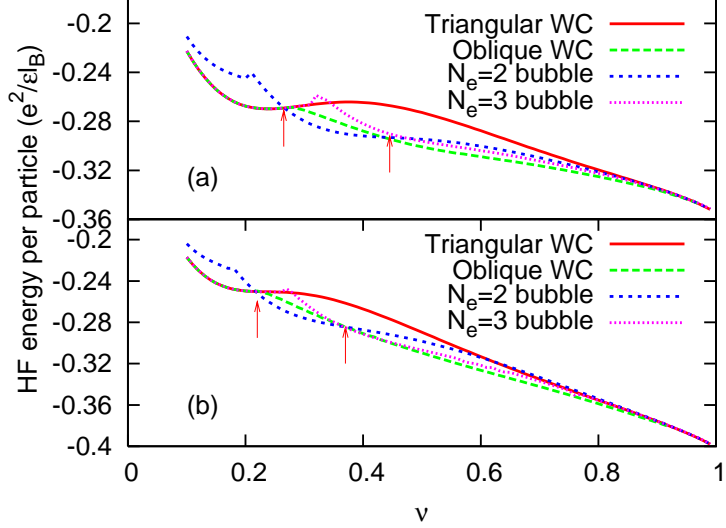


FIG. 5: (Color Online) Ground state energy per particle (measured in units of $e^2/\epsilon l_B$) for different crystal structures in the $n = 2$ Landau level for (a) graphene, and (b) a bilayer system at $d = 0$. The arrows mark critical filling factors ν^* at which transition from the triangular Wigner crystal to bubble crystal to anisotropic Wigner crystal take place.

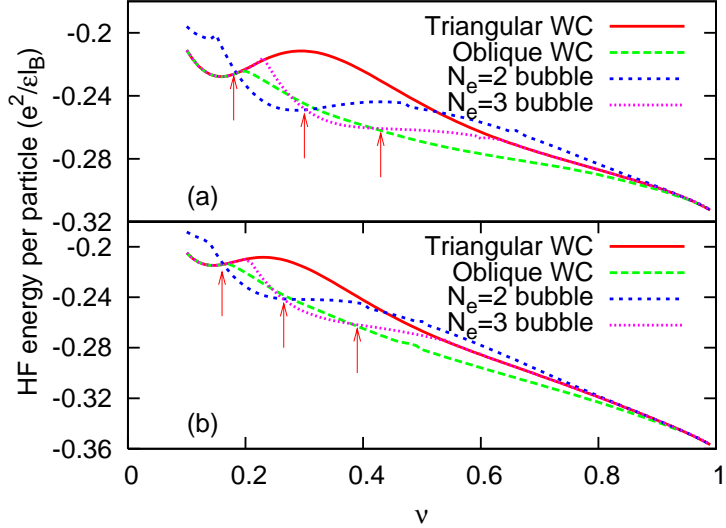


FIG. 6: (Color Online) Ground state energy per particle (measured in units of $e^2/\epsilon l_B$) for different crystal structures in the $n = 3$ Landau level for (a) graphene, and (b) a bilayer system at $d = 0$. The arrows mark critical filling factors ν^* at which transition from the triangular Wigner crystal to bubble crystal to anisotropic Wigner crystal take place.

quantum Hall system at $d = 0$ or a single layer system with vanishing Zeeman coupling). We showed that the (mean-field) ground state of graphene is evolves from a triangular Wigner crystal to an anisotropic Wigner crystal (striped state) as the partial filling ν in a given Landau level is increased. We also showed that for Landau level indices $n \geq 2$, a bubble crystal state with two electrons per unit cell, $N_e = 2$ occurs at intermediate values of ν . We have compared our results with mean-field results for a corresponding bilayer system at $d = 0$ (where the Coulomb interaction becomes isotropic in the pseudospin space). Our findings indicate that different form factors for electrons in graphene systematically shift the critical values of ν at which the phase transitions occur to higher values, *thus expanding the region of stability for the triangular Wigner crystal and bubble crystal states, compared to their counterparts in bilayer systems.*

These broken symmetry states in graphene are open to more probes than the conventional 2DEG. Our analysis predicts that anisotropies in the longitudinal resistance will be observed in high Landau levels (similar to those observed in quantum Hall systems) and will provide a signature of highly anisotropic Wigner crystal (striped) states.

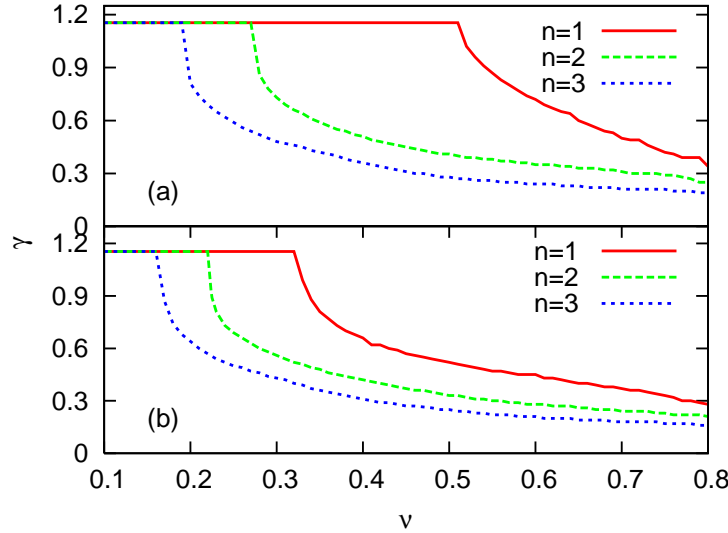


FIG. 7: (Color Online) Optimal crystal structure parameter $\gamma(\nu)$ for the ground state of (a) graphene and (b) bilayer system at $d = 0$ (bottom) for different Landau level indices. Recall that $\gamma = 2/\sqrt{3} = 1.15$ corresponds to a triangular lattice whereas $\gamma \leq 0.5$ corresponds to highly anisotropic Wigner crystals or striped states.

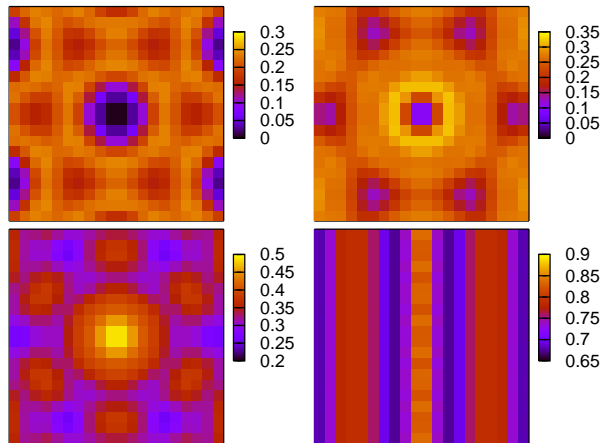


FIG. 8: (Color Online) A density plot for the ground state electron density in graphene with Landau level $n = 3$. Shown here are a triangular Wigner crystal at $\nu = 0.18$ (top left), a bubble state with $N_e = 2$ at $\nu = 0.25$ (top right), a bubble state with $N_e = 3$ that occurs at $\nu = 0.35$ (bottom left), and the anisotropic Wigner crystal state at $\nu = 0.75$ (bottom right).

In addition, since the 2DEG in graphene is literally at the surface, the electron density modulations can be directly probed, by scanning tunneling microscopy, and may provide a *direct* evidence of electronic crystal states in a 2DEG. Direct experimental observation of charge and current density distribution in quantum Hall systems is an outstanding problem; observation of isotropic Wigner crystal and striped states in graphene will improve our understanding of local structure of quantum Hall states.

VI. ACKNOWLEDGMENTS

It is a pleasure to thank Herb Fertig and Allan MacDonald for helpful discussions.

¹ E. Wigner, Phys. Rev. **46**, 1002 (1934).

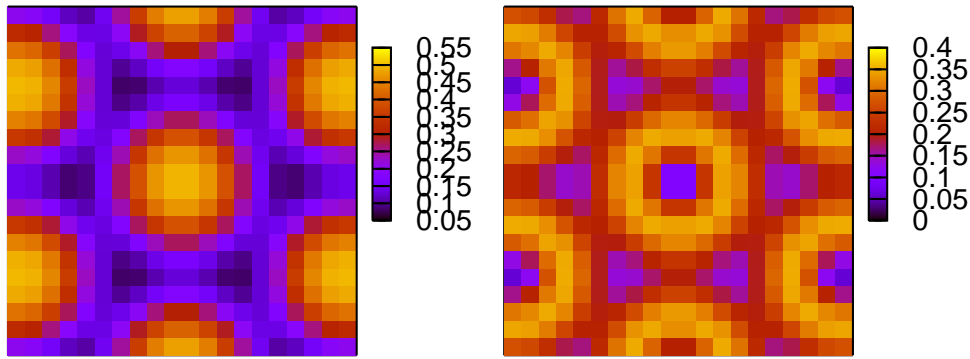


FIG. 9: (Color Online) A density plot of the ground state electron density profile in graphene (left) and bilayer system at $d = 0$ (right) at partial filling factor $\nu = 0.25$ in the $n = 1$ Landau level. Both systems have identical density matrices $\rho_n(\mathbf{q})$. However, the difference in the form factors in Eq. (20) leads to different real space densities.

- ² C. C. Grimes and G. Adams, Phys. Rev. Lett. **42**, 795 (1979).
- ³ E. Wigner, Phys. Rev. B **39**, 5005 (1989).
- ⁴ *Perspectives in quantum hall effects*, edited by Das Sarma and A. Pinczuk (Wiley and Sons, New York, 1997).
- ⁵ R. L. Willett, H. L. Stormer, D. C. Tsui, L. N. Pfeiffer, K. W. West, and K. W. Baldwin, Phys. Rev. B **38**, 7881 (1988).
- ⁶ M. P. Lilly, K. B. Cooper, J. P. Eisenstein, L. N. Pfeiffer, and K. W. West, Phys. Rev. Lett. **82**, 394 (1999).
- ⁷ P. R. Wallace, Phys. Rev. **71**, 622 (1947).
- ⁸ K. S. Novoselov *et al.*, Nature **438**, 197 (2005); Y. Zhang *et al.*, Nature **428**, 201 (2005).
- ⁹ H. P. Dahal, Y. N. Joglekar, K. S. Bedell, and A. V. Balatsky, Phys. Rev. B **74**, 233405 (2006).
- ¹⁰ G. W. Semenoff, Phys. Rev. Lett. **53**, 2449 (1984).
- ¹¹ F. D. M. Haldane, Phys. Rev. Lett. **61**, 2015 (1988).
- ¹² N. M. R. Peres, F. Guinea, and A. H. C. Neto, Phys. Rev. B **73**, 125411 (2005).
- ¹³ R. Côté and H. A. Fertig, Phys. Rev. B **62**, 1993 (2000).
- ¹⁴ A. M. Ettouhami, C. B. Doiron, F. D. Kliroonmos, R. Côté, and A. T. Dorsey, Phys. Rev. Lett. **96**, 196802 (2006).
- ¹⁵ M. O. Goerbig, R. Moessner, and B. Doucot, Phys. Rev. B **74**, 161407(R) (2006).
- ¹⁶ R. Côté and A. H. Macdonald, Phys. Rev. Lett. **65**, 2662(1990); Phys. Rev. B **44**, 8759(1991).
- ¹⁷ R. Côté, L. Brey, and A. H. MacDonald, Phys. Rev. B **46**, 10 239 (1992).
- ¹⁸ X. M. Chen and J. J. Quinn, Phys. Rev. B **45**, 11 054 (1992).
- ¹⁹ L. Brey and H. A. Fertig, Phys. Rev. B **62**, 10268 (2000).
- ²⁰ K. Yang, F. D. M. Haldane, and E. H. Rezayi, Phys. Rev. B **64**, 081301 (2001).